The hyperfine structure of the calcium monohalides

P. F. Bernath,[a] B. Pinchemel,[b] and R. W. Field

Spectroscopy Laboratory and Department of Chemistry, Massachusetts Institute of Technology, Cambridge, Massachusetts 02139

(Received 3 November 1980; accepted 4 February 1981)

Intermodulated fluorescence spectra of the $A\,^2\Pi - X\,^2\Sigma^+$ and $B\,^2\Sigma^+ - X\,^2\Sigma^+$ systems of $Ca^{79}Br$, $Ca^{81}Br$, and CaI have been recorded. ^{79}Br, ^{81}Br, and ^{127}I magnetic and electric quadrupole hyperfine structure was observed. The following parameters were determined (in MHz, 1σ uncertainties in parentheses):

	$Ca^{79}Br$	$Ca^{81}Br$	CaI
$X\,^2\Sigma^+$ b	90 (1)	98 (1)	116 (1) ,
$B\,^2\Sigma^+$ b	7 (1)	···	18 (1) ,
$B\,^2\Sigma^+$ eQq	< 3	···	− 66 (3) ,
$A\,^2\Pi$ eQq	31 (1)	28 (2)	− 55 (1) ,

with eQq set equal to zero in all $X\,^2\Sigma^+$ states. The observed hyperfine structure of CaF, CaCl, CaBr, and CaI may be interpreted in terms of halide orbital polarization rather than ionic–covalent mixing of M^+X^- and MX configurations.

I. INTRODUCTION

The first application of the technique of intermodulated fluorescence spectroscopy (IFS) to a diatomic molecular electronic transition was on isolated lines of the I_2 $B\,0_u^+ - X\,^1\Sigma_g^+$ system.[1] Since this initial demonstration, IFS has been applied to such molecules as NH_2,[2] BO_2,[3] CaCl,[4] CaF,[5] and VO.[6] We report here some results on the intermodulation spectra of the CaBr and CaI radicals.

Hyperfine structure of the $A\,^2\Pi - X\,^2\Sigma^+$ and $B\,^2\Sigma^+ - X\,^2\Sigma^+$ transitions has been observed for $^{40}Ca\,^{79}Br$, $^{40}Ca\,^{81}Br$, and $^{40}Ca\,^{127}I$. Hyperfine interactions within the X, A, and B electronic states were fit simultaneously in order to minimize correlations between molecular parameters for upper and lower electronic states. The addition of $A-X$ data to the fit allowed the determination of a magnetic hyperfine parameter for the $B\,^2\Sigma^+$ state of both CaBr and CaI. In this paper, the Frosch and Foley[7] a, b, and c magnetic hyperfine parameters are used.

The alkaline earth monohalides are a family of highly ionic molecules with the special attribute that all electrons but one reside in filled shells. Thus, it is tempting to interpret all observable properties (electronic energy levels, spin–orbit constants, Λ-doubling and spin–rotation splittings, hfs, and transition intensities) in terms of the properties of the single occupied, open-shell, mostly nonbonding, formally metal-centered orbital. The present hfs results probe the density and the gradient of the density of this metal-centered orbital *at the halogen nucleus*. Constrained by knowledge of other calcium monohalide molecular parameters, the hfs results permit estimates to be made of Ca^+ $s/p/d$ hybridization and X^- s and p polarization.

II. EXPERIMENT

The experimental arrangement was identical to that used for IFS of the CaF $A\,^2\Pi - X\,^2\Sigma^+$ system.[5] Calcium, entrained in argon, was reacted in a Broida-type flow system[8] with CH_3Br or CH_3CH_2I to form CaBr or CaI, respectively. Typical operating pressures were 0.5 Torr Ar to which < 1% oxidant was added via a concentric injector, just outside of the calcium oven.

The tunable, 1 MHz bandwidth laser used was a Coherent 699-21 ring dye laser pumped by 6–8 W of 514 nm radiation from a CR 18 argon ion laser. A dye mixture consisting of equal amounts of Rhodamine 101 and 6G covered the 610–650 nm spectral region at output power levels of 100–300 mW. The dye laser output was divided by a beam splitter into two beams of approximately equal intensity. One beam was mechanically chopped at 20 Hz, and the other at 1 kHz by a separate chopper. The two counterpropagating beams were directed, unfocused, through irises and, in a horizontal plane, through the vertical CaX flame. The power density of each beam in the fluorescence excitation and detection region was on the order of 100 mW cm^{-2}.

Fluorescence was detected, through a 10 nm bandpass interference filter centered at the laser wavelength, by a photomultiplier. The filters partly discriminated against weak chemiluminescence. Scattered laser light plus chemiluminescence amounted to typically 1% of the detected fluorescence intensity. Oxidants were selected to minimize chemiluminescence.

The fluorescence signal was input into two phase sensitive detectors, in series, as described for IFS on CaF.[5] The first (1 kHz) lock in was operated at 10 ms

---

[a] Present address: Herzberg Institute of Astrophysics, National Research Council of Canada, Ottawa, Canada K1A 0R6.

[b] Visiting scientist at MIT from Laboratoire de Spectroscopie des Molécules Diatomiques, Université des Sciences et Techniques, U.E.R. de Physique Fondamentale, 59655 Villeneuve d'Ascq, France.

 0021-9606/81/105508-08$01.00

time constant, the second (20 Hz) at 1 s, and the resultant IFS signal corresponded to typically 0.1% of the detected fluorescence intensity.

The hyperfine linewidths were 25–40 MHz, due mainly to power broadening. The natural linewidth is about 4 MHz for these molecules[9] and the onset of power broadening, calculated from

$$\mu E/h = (2\pi\tau)^{-1} ,$$

occurs near 20 mW cm^{-2}. At 0.5 Torr Ar, pressure broadening probably contributes 10 MHz. Stray magnetic fields from the 30 A ac current through the tungsten basket heater situated 6 cm from the fluorescence zone also broaden the IFS lines.

Absolute frequency calibration (± 0.003 cm^{-1}) was made by simultaneously recording CaX and I_2 excitation spectra.[10] A 300 MHz semiconfocal Fabry-Perot etalon provided relative frequency calibration (to ± 3 MHz for hyperfine components within a rotational line). Rotational assignments were made with reference to previous analyses of CaBr[11] and CaI[12] spectra.

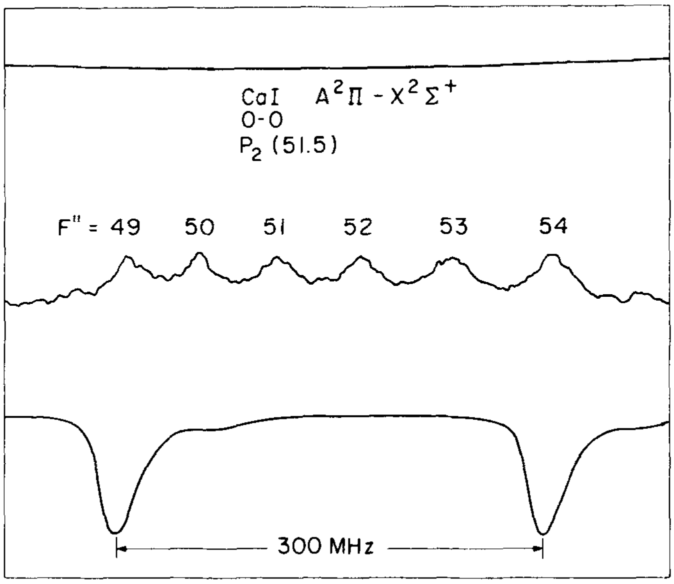

FIG. 2. Intermodulated fluorescence spectrum of the CaI $A\,^2\Pi$–$X\,^2\Sigma^+$ 0–0 P_2 (51.5) line. The asymmetry produced by the quadrupole interaction is more evident than in Fig. 1.

III. RESULTS

For CaBr, the nuclear spin of ^{79}Br or ^{81}Br is 3/2; thus, four strong $\Delta F = \Delta J$ hyperfine lines are expected for each $J \geq 3/2$ rotational line. Figure 1 shows the hfs pattern observed for the P_{12} (64.5) line of the $A\,^2\Pi$–$X\,^2\Sigma^+$ 0–0 band. At such high J one would expect four equidistant lines if the only significant contribution to hfs were magnetic hyperfine in the $X\,^2\Sigma^+$ state. The $A\,^2\Pi$ state should follow Hund's case a_β coupling, so its magnetic hfs decreases as $1/J$ and ought to be negligible[5] at $J=63.5$. The Hund's $b_{\beta J}$ coupling[13] of $X\,^2\Sigma^+$ would result in a constant hfs splitting of $b/2$ at high J. In fact, the hfs components are not equally spaced; this indicates the presence of electric quadrupole contributions to X and/or A state hfs.

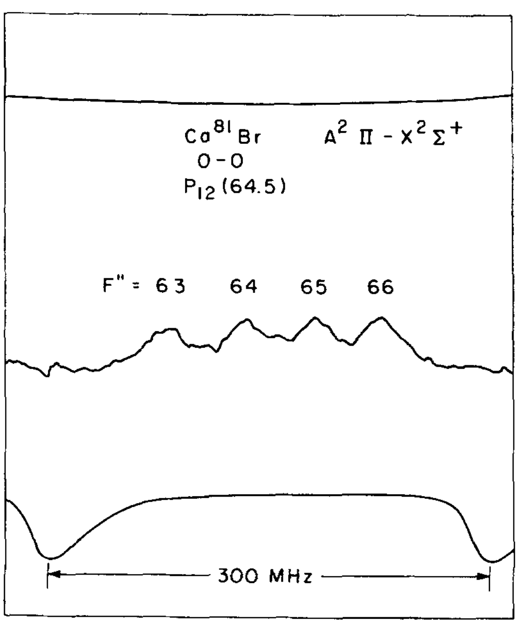

FIG. 1. Intermodulated fluorescence spectrum of the Ca^{81}Br $A\,^2\Pi$–$X\,^2\Sigma^+$ 0–0 P_{12} (64.5) line. The top trace is part of the Doppler-broadened line, the middle trace is the Doppler-free spectrum, and the bottom trace shows frequency markers from a 300 MHz Fabry–Perot interferometer.

This effect is more pronounced in the CaI $A\,^2\Pi$–$X\,^2\Sigma^+$ 0–0 P_2(51.5) line illustrated by Fig. 2. The ^{127}I nucleus has spin of 5/2, so there are six strong hfs lines. However, the electric quadrupole moment of ^{127}I is about a factor of 2 larger and has opposite sign than for ^{79}Br and ^{81}Br.[14] As a result, the hfs of CaI exhibits larger deviations (and in the opposite sense) from equidistant spacing than CaBr.

The spectra of CaBr and CaI are extremely congested due to overlapping sequences and branches and the presence of two approximately equally abundant Br isotopes. This means that, even with sub-Doppler resolution, only a few branches could be examined for hfs. These branches are $A\,^2\Pi_{1/2}$–$X\,^2\Sigma^+$ 0–0 and 1–1 $P_{12}(J)$ (Ca^{81}Br, 14 lines; Ca^{79}Br, 11 lines; CaI, nine lines), $A\,^2\Pi_{3/2}$–$X\,^2\Sigma^+$ 0–0 and 1–1 $P_2(J)$ (Ca^{81}Br, nine lines; Ca^{79}Br, 10 lines; CaI, nine lines), $B\,^2\Sigma^+$–$X\,^2\Sigma^+$ 0–0 and 0–1 $P_1(N)$ (Ca^{79}Br, 14 lines; CaI, five lines). Tables I and II contain all of the splittings for lines of the A–X and B–X transitions that were examined for hfs in CaBr, while Table III lists the CaI results. The splittings are tabulated as differences between adjacent components, starting from the red and progressing to higher frequency. In the case of the $B\,^2\Sigma^+$–$X\,^2\Sigma^+$ $P_1(N'')$ branch, the differences $D0$ to $D4$ and $D\Sigma$ are

$$D0 = E'(F' = N'' + 1) - E'(N'' + 2) + E''(F'' = N'' + 3) - E''(N'' + 2) , \quad (1a)$$

$$D1 = E'(N'') - E'(N'' + 1) + E''(N'' + 2) - E''(N'' + 1) , \quad (1b)$$

$$D2 = E'(N'' - 1) - E'(N'') + E''(N'' + 1) - E''(N'') , \quad (1c)$$

$$D3 = E'(N'' - 2) - E'(N'' - 1) + E''(N'') - E''(N'' - 1) , \quad (1d)$$

TABLE I. $Ca^{79}Br$ hyperfine splittings (in MHz).[a]

Band	Assignment	$D1$	$D2$	$D3$	$D\Sigma$
$B\,^2\Sigma^+-X\,^2\Sigma^+$					
0–1	$P_1(25)$	41(0)	44(−3)	41(1)	126(−2)
0–1	$P_1(27)$	41(0)	41(0)	39(3)	121(3)
0–1	$P_1(28)$	42(−1)	41(0)	39(3)	122(2)
0–1	$P_1(32)$	39(2)	46(−4)	42(0)	127(−2)
0–1	$P_1(33)$	42(−1)	43(−1)	39(3)	124(1)
0–1	$P_1(34)$	43(−2)	40(2)	43(−1)	126(−1)
0–1	$P_1(35)$	43(−2)	42(0)	43(−1)	128(−3)
0–1	$P_1(58)$	43(−2)	40(2)	44(−2)	127(−2)
0–1	$P_1(59)$	42(−1)	43(−1)	40(2)	125(0)
0–1	$P_1(60)$	42(−1)	43(−1)	43(−1)	128(−3)
0–1	$P_1(61)$	44(−3)	40(2)	40(2)	124(−1)
0–1	$P_1(65)$	40(2)	41(1)	42(0)	123(3)
0–1	$P_1(66)$	40(2)	41(1)	39(3)	120(6)
0–1	$P_1(68)$	42(0)	45(−3)	38(4)	125(1)
$A\,^2\Pi_{1/2}-X\,^2\Sigma^+$					
0–0	$P_{12}(5.5)$	50(−3)	48(1)	31(−5)	129(−7)
0–0	$P_{12}(7.5)$	54(1)	47(1)	30(−6)	131(−4)
0–0	$P_{12}(9.5)$	52(−1)	44(−2)	34(−3)	130(−6)
1–1	$P_{12}(15.5)$	54(1)	41(−5)	35(−2)	130(−6)
0–0	$P_{12}(18.5)$	52(−1)	46(1)	33(−4)	131(−4)
0–0	$P_{12}(24.5)$	49(−4)	45(0)	34(−3)	128(−7)
0–0	$P_{12}(25.5)$	55(2)	47(2)	41(4)	143(8)
1–1	$P_{12}(27.5)$	50(−3)	41(−4)	36(−1)	127(−8)
0–0	$P_{12}(59.5)$	51(−2)	46(1)	36(−1)	133(−2)
0–0	$P_{12}(63.5)$	52(−1)	45(0)	39(2)	136(1)
0–0	$P_{12}(69.5)$	48(−5)	44(−1)	35(−2)	127(−8)
$A\,^2\Pi_{3/2}-X\,^2\Sigma^+$					
0–0	$P_2(13.5)$	52(0)	45(−1)	37(0)	134(−1)
0–0	$P_2(18.5)$	53(0)	45(0)	34(−3)	132(−3)
0–0	$P_2(24.5)$	53(0)	49(4)	38(1)	140(5)
0–0	$P_2(25.5)$	53(0)	49(4)	36(−1)	138(3)
0–0	$P_2(34.5)$	53(0)	50(5)	44(7)	147(12)
0–0	$P_2(46.5)$	54(1)	43(−2)	38(1)	135(−1)
0–0	$P_2(58.5)$	58(5)	50(5)	37(0)	145(10)
0–0	$P_2(59.5)$	56(3)	43(−2)	42(5)	141(6)
0–0	$P_2(76.5)$	50(−3)	47(2)	40(3)	137(2)
0–0	$P_2(77.5)$	51(−2)	49(4)	41(4)	141(6)

[a]Obs.−calc. in parentheses.

$$D4 = E'(N''-3) - E'(N''-2) + E''(N''-1) + E''(N''-2)\ , \tag{1e}$$

$$D\Sigma = \Sigma Di = E'(F'_{\min}) - E'(F'_{\max}) + E''(F''_{\max}) - E''(F''_{\min})\ . \tag{1f}$$

For the $A\,^2\Pi - X\,^2\Sigma^+$ transition, the $P_{12}(J''=N''-\frac{1}{2})$ and $P_2(J''=N''-\frac{1}{2})$ branches originate from the f parity component of the $X\,^2\Sigma^+$ state, so the order of the F quantum numbers is reversed[13]:

$$D0 = E'(F'=N''-4) - E'(N''-3) + E''(F'=N''-2) - E''(N''-3)\ , \tag{2a}$$

$$D1 = E'(N''-3) - E'(N''-2) + E''(N''-1) - E''(N''-2)\ , \tag{2b}$$

$$D2 = E'(N''-2) - E'(N''-1) + E''(N'') - E''(N''-1)\ , \tag{2c}$$

$$D3 = E'(N''-1) - E'(N'') + E''(N''+1) - E''(N'')\ , \tag{2d}$$

$$D4 = E'(N'') - E'(N''+1) + E''(N''+2) - E''(N''+1)\ , \tag{2e}$$

$$D\Sigma = E'(F'_{\min}) - E'(F'_{\max}) + E''(F''_{\max}) - E''(F''_{\min})\ . \tag{2f}$$

In taking differences of adjacent hfs components, the extreme red and blue components of a rotational line are used only once. Their measured difference $D\Sigma$ was included in the fit so that *each* component would be used twice in the measured differences.

The model used to fit the results is based on the Frosch and Foley[7] Hamiltonian

$$H_{\mathrm{hfs}} = a\Lambda \mathbf{I}\cdot\mathbf{k} + b\mathbf{I}\cdot\mathbf{S} + c(\mathbf{I}\cdot\mathbf{k})(\mathbf{S}\cdot\mathbf{k}) + eQq\,[3I_z^2 - I(I+1)]/4I(2I-1)\ . \tag{3}$$

In the case of $^2\Sigma$ states, it is possible to derive exact analytical expressions for the hyperfine splittings.[15] For the $X\,^2\Sigma^+$ state, it is necessary to use these expressions since there is a transition from case $b_{\beta S}$ to $b_{\beta J}$ as N increases.[5] The hyperfine Hamiltonian matrix shown in Table IV is very similar to Radford's.[15] The off-diagonal electric quadrupole term is too small to affect the energy levels of CaBr and CaI so it has been eliminated. The resultant 2×2 matrix is exactly diagonalized and the resultant energy level expressions used without further algebraic simplification.

In the CaBr and CaI $B\,^2\Sigma^+$ states the spin–rotation constants are much larger than in $X\,^2\Sigma^+$ (see Table V). The separation between electron–spin components ($J=N\pm\frac{1}{2}$) is always at least 10 times larger than hfs splittings and $\Delta J=\pm 1$ interaction terms (case $b_{\beta J}$); thus, only the diagonal elements ($\Delta J=0$) of the hyperfine matrix were used in the least-squares fits.

The $A\,^2\Pi$ states were assumed to obey a_β type coupling, with hyperfine energy levels described by[13]

TABLE II. $Ca^{81}Br$ hyperfine splittings (in MHz).[a]

Band	Assignment	$D1$	$D2$	$D3$	$D\Sigma$
$A\,^2\Pi_{1/2}-X\,^2\Sigma^+$					
0–0	$P_{12}(3.5)$	57(0)	47(−2)	39(2)	143(0)
0–0	$P_{12}(4.5)$	57(−1)	47(−3)	38(−1)	142(−5)
0–0	$P_{12}(5.5)$	57(−1)	58(8)	33(−7)	142(0)
0–0	$P_{12}(7.5)$	62(5)	48(−2)	31(−10)	153(13)
0–0	$P_{12}(9.5)$	62(5)	49(−1)	36(−5)	147(−1)
0–0	$P_{12}(12.5)$	55(−2)	52(2)	40(−1)	147(−1)
1–1	$P_{12}(15.5)$	56(−1)	48(−2)	38(−3)	142(−6)
0–0	$P_{12}(18.5)$	56(0)	51(1)	41(−1)	148(0)
0–0	$P_{12}(24.5)$	51(−5)	48(−2)	42(0)	141(−7)
0–0	$P_{12}(25.5)$	57(1)	49(0)	42(0)	148(1)
1–1	$P_{12}(27.5)$	55(−1)	45(−4)	40(−2)	140(−7)
0–0	$P_{12}(64.5)$	56(0)	49(0)	43(1)	148(1)
0–0	$P_{12}(70.5)$	56(0)	48(−1)	41(−1)	145(−2)
0–0	$P_{12}(84.5)$	57(1)	53(4)	42(0)	152(5)
$A\,^2\Pi_{3/2}-X\,^2\Sigma^+$					
0–0	$P_2(13.5)$	60(4)	47(−3)	43(1)	150(2)
0–0	$P_2(24.5)$	60(4)	50(1)	43(1)	153(6)
0–0	$P_2(34.5)$	56(0)	48(−1)	45(3)	149(2)
0–0	$P_2(47.5)$	56(0)	51(2)	49(7)	156(9)
0–0	$P_2(48.5)$	54(−2)	48(−1)	44(2)	146(−1)
0–0	$P_2(59.5)$	56(0)	49(0)	44(2)	149(2)
0–0	$P_2(60.5)$	55(−1)	49(0)	43(1)	147(0)
0–0	$P_2(77.5)$	53(−3)	51(2)	49(7)	153(6)
0–0	$P_2(78.5)$	57(1)	50(1)	42(0)	149(2)

[a]Obs.−calc. in parentheses.

TABLE III. CaI hyperfine splittings.[a]

Band	Assignment	$D0$	$D1$	$D2$	$D3$	$D4$	$D\Sigma$
$B\,^2\Sigma^+-X\,^2\Sigma^+$							
0–1	$P_1(24)$	41(– 2)	44(1)	49(1)	55(– 1)	49(– 1)	238(– 2)
0–1	$P_1(53)$	40(– 1)	44(0)	52(– 3)	53(1)	57(1)	246(– 2)
0–1	$P_1(54)$	42(– 4)	44(0)	48(1)	54(0)	57(1)	245(– 2)
0–0	$P_1(62)$	39(0)	44(0)	48(1)	53(1)	59(– 1)	243(1)
0–0	$P_1(65)$	42(– 3)	46(– 2)	49(0)	59(– 5)	65(– 7)	261(– 17)
$A\,^2\Pi_{1/2}-X\,^2\Sigma^+$							
0–0	$P_{12}(15.5)$	52(4)	58(– 4)	55(– 2)	61(– 1)	66(– 2)	292(– 5)
0–0	$P_{12}(17.5)$	49(– 1)	56(4)	51(– 6)	66(4)	66(– 2)	288(– 1)
0–0	$P_{12}(26.5)$	48(– 1)	54(1)	57(0)	63(1)	65(– 3)	287(– 2)
0–0	$P_{12}(27.5)$	48(– 1)	53(0)	59(2)	62(0)	65(– 3)	287(– 2)
0–0	$P_{12}(46.5)$	48(1)	51(– 3)	59(– 2)	64(– 1)	69(2)	291(– 3)
0–0	$P_{12}(51.5)$	46(– 3)	50(– 3)	58(0)	57(– 5)	68(1)	279(– 10)
0–0	$P_{12}(56.5)$	48(– 1)	52(– 1)	56(– 2)	61(– 1)	68(1)	285(– 4)
0–0	$P_{12}(58.5)$	49(0)	49(– 4)	57(– 1)	61(– 1)	66(– 1)	282(– 7)
0–0	$P_{12}(61.5)$	52(3)	58(5)	60(2)	60(– 2)	78(11)	308(19)
$A\,^2\Pi_{3/2}-X\,^2\Sigma^+$							
0–0	$P_2(8.5)$	49(2)	49(2)	59(3)	63(2)	64(– 4)	284(5)
0–0	$P_2(9.5)$	50(3)	52(1)	58(2)	63(2)	69(1)	292(9)
0–0	$P_2(19.5)$	56(8)	53(1)	58(1)	65(3)	66(– 2)	298(11)
0–0	$P_2(30.5)$	55(7)	48(– 5)	59(2)	63(1)	68(1)	293(6)
1–1	$P_2(38.5)$	47(– 2)	53(0)	58(1)	61(– 1)	67(0)	286(– 2)
0–0	$P_2(40.5)$	46(– 3)	56(3)	57(0)	61(– 1)	68(1)	288(0)
0–0	$P_2(51.5)$	48(– 1)	56(3)	58(1)	63(1)	69(2)	294(6)
0–0	$P_2(55.5)$	44(– 5)	53(0)	57(– 1)	62(0)	65(– 2)	281(– 8)
1–1	$P_2(68.5)$	49(1)	50(– 3)	58(0)	62(0)	70(3)	289(1)

[a]Obs.–calc. in parentheses.

$$E_{a_\beta}(J,\Omega,\Sigma,F)=[a+(b+c)\Sigma]\Omega C(F,I,J)/2J(J+1)\ , \qquad (4)$$

where $C(F,I,J)$ is defined in Table IV. The electric quadrupole hfs is given by

$$W_Q=-eQqY(F,J,I)[1-3\Omega^2/J(J+1)]\ , \qquad (5)$$

where $Y(F,J,I)$ is Casimir's function.[14]

Equation (4) neglects an e/f parity-dependent contribution to the hyperfine splitting in the $\Omega=1/2$ component of $A\,^2\Pi$:

$$\pm\frac{d(J+1/2)}{2J(J+1)}\mathbf{I}\cdot\mathbf{J}\ .$$

The magnetic hyperfine splitting is altered by equal and opposite amounts for e vs f levels. At high J values, the hfs splittings of the e and f levels should differ by d. When d was fixed at zero, no systematic e/f residuals were observed at high J values in either $A\,^2\Pi_{1/2}$ or $A\,^2\Pi_{3/2}$ spin components for both CaBr and CaI. This implies an upper limit of

$$|d|<6\text{ MHz}\ .$$

Equation (4) also neglects hyperfine matrix elements off diagonal in Ω. At the highest J values sampled, where the effect of $\Delta\Omega=\pm1$ interactions should be most important, the second-order perturbation cross term between $\mathbf{I}\cdot\mathbf{J}$ and $B\,\mathbf{S}\cdot\mathbf{J}$ contributes less than 10% as much to the magnetic hfs as the $\Delta\Omega=0$ matrix elements represented by Eq. (4). Thus, Eqs. (4) and (5) provide a satisfactory representation of the hfs in the $A\,^2\Pi$ states of the calcium monohalides.

The splittings listed in Tables I–III were input to nonlinear, least-squares fits. All hfs splittings for both $A-X$ and $B-X$ systems were fit simultaneously. Lines from 0–0, 1–1, and 0–1 vibrational bands were included since no vibrational dependence of hfs parameters could be detected at the precision (± 3 MHz) of the present IFS spectra. Childs and Goodman[16] found that the magnetic

TABLE IV. Hyperfine Hamiltonian for the $F_1(e)$ and $F_2(f)$ components of a given N of a $^2\Sigma^+$ state.[a]

	$e\ (J=N+\frac{1}{2})$	$f\ (J=N-\frac{1}{2})$
e	$\left[b+\frac{c}{2N+3}\right]\frac{C(F,I,J)}{2(2N+1)}+W_Q+\frac{\gamma N}{2}$	$\left[b+\frac{c}{2}\right]\frac{E(F,I,N)}{2(2N+1)}$
f	sym	$\left[-b+\frac{c}{2N-1}\right]\frac{C(F,I,J)}{2(2N+1)}+W_Q-\frac{\gamma(N+1)}{2}$

[a]$C(F,I,J)=F(F+1)-I(I+1)-J(J+1)$. $E(F,I,N)=[(F+N-I+1/2)(F-N+I+1/2)(F+N+I+3/2)(-F+N+I+1/2)]^{1/2}$. $W_Q=-eQq[3C(C+1)/4-I(I+1)J(J+1)]/8I(2I-1)J(J+1)$.

TABLE V. Fine and hyperfine structure of calcium halides for $v = 0$ (in MHz). One σ uncertainties in parentheses.

		CaF[a]	$Ca^{35}Cl$	$Ca^{79}Br$	$Ca^{81}Br$	CaI
$X\,^2\Sigma^+$	γ	39.505	41(2)[b]	90.1[e]	89.4[e]	168(1)[f]
	b	108.491	30[c]	90(1)	98(1)	116(1)
	c	39.476	...	...[d]	...[d]	...[d]
	b/g_I	20.635	55	64(1)	65(1)	103(1)
$B\,^2\Sigma^+$	γ	−1374(1)[g]	−1965(2)[h]	−2069(1)[e]	−2052(1)[e]	−4202(10)[f]
	b	...	...	7(1)	...	18(1)
	eQq[i]	...	...	0(< 3 MHz)	...	−66(3)
	b/g_I	...	...	5(1)	...	16(1)
$A\,^2\Pi$	eQq[i]	...	...	31(1)	28(2)	−55(1)

[a]Reference 16.
[b]P. J. Domaille, T. C. Steimle, and D. O. Harris, J. Mol. Spectrosc. 66, 503 (1977).
[c]Reference 19.
[d]Set to zero in the fits.
[e]Reference 11.
[f]Reference 12.
[g]M. Dulick, P. F. Bernath, and R. W. Field, Can. J. Phys. 58, 703 (1980).
[h]L. E. Berg, L. Klynning, and H. Martin, Phys. Scr. 22, 216 (1980).
[i]eQq'' of $X\,^2\Sigma^+$ set to zero in the fits. Constants given are actually $\Delta eQq(B-X)$ and $\Delta eQq(A-X)$.

hfs of CaF $X\,^2\Sigma^+$ decreased by 0.85% as v increased by one. A similar hfs variation for CaBr or CaI would have been undetectable here. The precision of the radio frequency measurements[17] was 3×10^3 higher than the present IFS results.

In all, the hyperfine Hamiltonian for the X, A, and B states involves 11 independent parameters: b, c, eQq, and γ for both the X and B states; and a, $(b+c)$, and eQq for the A state. The present data set is inadequate in both precision and extent to determine all 11 parameters. Some of these parameters, such as c in the $B\,^2\Sigma^+$ state should be undetectably small[5]; others, such as the three eQq parameters, should be partly correlated, even if data from more than one branch were available.[18] The contribution of the c parameter to the X and B state hfs varies as N^{-1}, and, since low-N data were unobtainable, was fixed at zero in the fits. The a and $(b+c)$ parameters for $A\,^2\Pi$ were set to zero for the same reason. The correlation of eQq parameters was artificially broken by setting $eQq''=0$ for the $X\,^2\Sigma^+$ states. This means, in effect, that the parameters $\Delta eQq(A-X)$ and $\Delta eQq(B-X)$ are being determined. The remaining parameters b in the $^2\Sigma^+$ states and eQq in the $A\,^2\Pi$ and $B\,^2\Sigma^+$ states were determined and their values are listed in Table V. The values of γ for the X and B states were fixed at their known values.[11,12] The previously determined CaF[17] and CaCl[19] constants are included for comparison.

As a check of the parameters obtained, the $Ca^{81}Br$ constants can be predicted from those of $Ca^{79}Br$ using the known ratio of nuclear moments.[14] For the $X\,^2\Sigma^+$ state, the predicted and observed values are 97(1) and 98(1) MHz, respectively. For eQq (actually ΔeQq) of the $A\,^2\Pi$ state, the predicted and observed $Ca^{81}Br$ values are 26(1) and 28(2) MHz, respectively.

IV. DISCUSSION

In this section, the observed hfs parameters will be used to construct a simple model for the electronic structure of the calcium monohalides. The unique feature of these highly ionic molecules is that, in zeroth order, only one electron resides outside of filled Ca^{+2} and X^- shells. All known CaX electronic transitions correspond to promotions of this electron between nonbonding, metal-centered orbitals. Since virtually all observable properties of CaX molecules should be predominantly determined by the form of the occupied nonbonding orbital, one has an unusual opportunity to characterize such orbitals.

The halide nuclear spin acts as a probe of the size and shape of the unpaired spin-density present at the halide nucleus. The strongest indication that the CaX molecules are nearly perfectly M^+X^- ionic is that the magnitudes of the magnetic hyperfine parameters (b's) are less than 1% of the values calculated for neutral halogen atoms.[20] This is consistent with almost complete localization of the unpaired spin density on the Ca^+.

The hfs of such highly ionic molecules can be viewed as arising via two distinct mechanisms: (1) A small amount of covalent character is present by $Ca^+X^-\sim CaX$ configuration interaction, and (2) the X^- orbitals are polarized by the unpaired electron on Ca^+ (spin polarization).[21] Mechanism (1) requires net formal electron transfer from X^- to Ca^+, while (2) preserves the formally closed-shell character of X^-. A convenient feature of mechanism (2) is that all relevant matrix elements may be estimated using M^+ and X^- atomic orbitals. It will be shown that mechanism (2) accounts for the major part of the CaX hfs.

The b parameter (Fermi contact term) is related to the spin density at the halide nucleus through the equation[7]

$$b = g_I \mu_0 \mu_N \left[\frac{16\pi}{3} |\psi(0)|^2 - \left\langle \frac{3\cos^2\chi - 1}{r^3} \right\rangle \right] , \qquad (6)$$

where g_I is the X nuclear magnetic moment, μ_0 and μ_N are the electron and nuclear magneton, $\psi(0)$ is the amplitude of the electron spin density at the X nucleus, r is the e^- to X-nucleus separation, χ is the angle between $\mathbf{r}$ and the M^+–X^- axis, and $\langle\ \rangle$ implies expectation value. The first problem is to separate out the $\psi(0)$ part of b. If the c parameter were known

$$c = 3g_I \mu_0 \mu_N \langle (3\cos^2\chi - 1)/r^3 \rangle , \qquad (7a)$$

then one could define

$$b_{\mathrm{iso}} = b + c/3 , \qquad (7b)$$

where b_{iso} is directly proportional to $|\psi(0)|^2$. For CaF $X\,^2\Sigma^+$, the known value[16] of c allows calculation of

$$b_{\mathrm{iso}} = 121.6 \text{ MHz} .$$

In this case b and b_{iso} differ by only 12%. Fortunately, one expects the c constant to be sufficiently small for all of the CaX molecules that

$$b_{\mathrm{iso}} \approx b$$

will give a good approximation to $|\psi(0)|^2$. Table V lists known values of b/g_I for the X, A, and B states of CaF, $Ca^{35}Cl$, $Ca^{79}Br$, $Ca^{81}Br$, and CaI so that spin densities may be directly compared. It will be suggested below that the fivefold increase in $|\psi(0)|^2$ for $X\,^2\Sigma^+$ from CaF to CaI results from mainly the increasing spin polarization of the halogen, not from an increase in covalent character.

The model used here to explain the magnetic hfs in the $B\,^2\Sigma^+$ and $X\,^2\Sigma^+$ states is a generalization of one used by Dagdigian, Cruse, and Zare[9] and by Knight *et al.*[22] It combines the idea of $s/p/d$ mixing of Ca^+ orbitals[9,22] with a (zero free parameter) renormalization effect discussed by Freeman and Watson,[21] which mixes in a small amount of X^- ns character into the singly occupied open-shell molecular orbital.

One starts by writing the CaX molecular orbitals in terms of linear combinations of Ca^+ atomic orbitals. The X^- ion provides a ligand field which mixes atomic orbitals of different nl values and also splits these orbitals into the σ, π, and δ forms appropriate to the $C_{\infty v}$ point group. One obtains for molecular orbital shapes

$$\psi(B\,^2\Sigma^+) = e\,|4p\sigma(Ca^+)\rangle - (1-e^2)^{1/2}\,|3d\sigma(Ca^+)\rangle , \qquad (8a)$$

$$\psi(A\,^2\Pi) = f\,|4p\pi(Ca^+)\rangle - (1-f^2)^{1/2}\,|3d\pi(Ca^+)\rangle , \qquad (8b)$$

$$\psi(X\,^2\Sigma^+) = g\,|4s\sigma(Ca^+)\rangle - (1-g^2)^{1/2}\,|4p\sigma(Ca^+)\rangle . \qquad (8c)$$

Note that $4s\sigma$ and $3d\sigma$, respectively, are artificially (but inconsequentially) excluded from B and X state wave functions. The e, f, and g mixing coefficients are to be determined from measured molecular parameters such as radiative lifetimes, Λ doubling, spin–rotation, spin–orbit, and hfs constants.

It is easy to show that Eq. (8c) is inadequate to explain the magnetic hyperfine structure. Representing each atomic orbital by a single Slater type orbital, with the exponents chosen by Burns' rules,[23] one can calculate $|\psi(r_X)|^2$. Burns' rules were formulated to reproduce Hartree–Fock moments of r (orbital shapes) rather than minimize the total orbital energy. Using Eq. (6), the predicted magnetic hfs is more than a factor of 10 too small for all $X\,^2\Sigma^+$ states.

Following Freeman and Watson,[21] the molecular wave functions are now augmented by a small amount of ns halide character $-(S+\lambda)|ns\,X^-\rangle$. Although Freeman and Watson show that halide orbitals in addition to the valence halide orbitals should be included, for simplicity inner orbital contributions will be neglected. The coefficient λ is interpreted as a covalency parameter while S is a measure of halide spin–orbital polarization. *The S contribution can be considered to originate solely from the nonorthogonality of the atomic* Ca^+ *and* X^- *basis orbitals.* A reasonable estimate for S is thus the orbital overlap integral between the Ca^+ and X^- basis functions.[21] Orbital overlap integrals for Slater-type functions are tabulated.[24] Burns' rules[23] were used to determine the orbital exponents for the single-ζ, Slater-type basis functions for valence Ca^+ and X^- orbitals.

The covalency parameter λ must also be estimated. It is reasonable to set $\lambda = 0$ for the entire CaX series. This may seem surprising in reference to the traditional ionicity index[25] R_e/R_x. R_e and R_x are, respectively, the equilibrium internuclear distance and the hypothetical internuclear distance at which the bound ionic potential curve crosses the nonbonding neutral curve. When $1.5 < R_e/R_x < 2$, as it is only for CaI (1.67), bonding is expected to be mostly ionic, but with some covalent character.

The following facts suggest that λ is negligibly small, even for CaI: (1) The Rittner ionic model[26] accurately reproduces the $X\,^2\Sigma^+$ state dissociation energies[27] of the calcium monohalides. (2) The spin–orbit constant A of $A\,^2\Pi$ changes monotonically from 71.45 cm^{-1} in CaF[28] to 45.8 cm^{-1} for CaI.[12] (These A values are corrected using unique perturber estimates of the o parameter.[29] Without this correction, A ranges from 72.60 cm^{-1} for CaF to 60.12 cm^{-1} for CaI.) About half of the change in A can be accounted for by the increasing d character $(F \to I)$ of the molecular orbital. The remainder is consistent with $\lambda \approx 0.05$ (about 0.25% covalent character), a value that is nearly independent of halide. This argument depends on the assumption that the X, A, and B states all have similar λ values. The small differences in R_e and ω_e values between these states[28] supports this assumption. (3) The conventional correlation between ionicity and electronegativity differences (Ref. 14, p. 582) suggests 11% covalent character ($\lambda \approx 0.33$) for the CaI $X\,^2\Sigma^+$ state. This would imply, if λ were identical for the $A\,^2\Pi$ state, a spin–orbit constant $A = -500$ cm^{-1}!

The above arguments demonstrate that λ is small. It will now be shown that even a small value of λ leads to contradictory interpretations of the magnetic and electric quadrupole hfs. The decrease, by almost an order of magnitude, of the magnetic hyperfine b parameter from the $X\,^2\Sigma^+$ to the $B\,^2\Sigma^+$ state of CaBr would normally be explained by a *decrease* in λ. In contrast, the value of eQq is the same in the B and X states of CaBr and actually larger in absolute magnitude in the B vs X state of CaI, thus suggesting[14] either no change or an *increase* in λ. The simplest way out of this quandary is to set $\lambda = 0$ and attempt to explain the hfs entirely by spin polarization.

It is not surprising that the usual correlation[14] between eQq and the λ ionicity parameter breaks down for the alkaline earth monohalides. These molecules are unique in that they have an odd total number of electrons and that the odd electron is located predominantly on the nucleus without spin. This means that hfs is determined by a delicate balance of weakly sampled large effects, in contrast to the more usual situation when valence orbitals all contain an even number of electrons or the odd electron is formally associated with the $I > \frac{1}{2}$ nucleus.

The first step in explaining the hfs in terms of the spin-polarization model is to use the magnetic hfs to obtain an estimate of S, the overlap integral of the unique Ca^+ centered orbital with one of the filled-shell X^- orbitals. Equations (6) and (8) and the suggested[21] admixed $-S\,|ns\,X^-\rangle\, ns$ halide character lead to

$$b/g_I \doteq 800\, S^2 |\phi_{nsX^-}(0)|^2 \; , \qquad (9)$$

where $|\phi_{nsX^-}(0)|^2$ is the charge density (in atomic units) of the halide ns orbital at the halide nucleus and b/g_I is in MHz. The overlap integrals S for the $X\,^2\Sigma^+$ and $B\,^2\Sigma^+$ states are

$$S_X = gS\,[4s\sigma(Ca^+),\, ns\sigma(X^-)] - (1-g^2)^{1/2} S[4p\sigma(Ca^+),\, ns\sigma(X^-)] \; , \qquad (10a)$$

$$S_B = eS\,[4p\sigma(Ca^+),\, ns\sigma(X^-)] - (1-e^2)^{1/2} S\,[3d\sigma(Ca^+),\, ns\sigma(X^-)] \; . \qquad (10b)$$

Values of $|\phi_{nsX^-}(0)|^2$ were taken from Hartree–Fock calculations of Froese-Fischer[30] (on neutral atoms). Equations (10) were then solved for the mixing coefficients g and e using overlap integrals between Ca^+ and X^- atomic orbitals for which Burns' rule ζ values were selected. The mixing fractions obtained are listed in Table VI.

The magnetic hfs of the $X\,^2\Sigma^+$ state for the CaX molecules suggests that 25%–35% $4p\sigma(Ca^+)$ character is admixed with $4s\sigma(Ca^+)$ into the lowest energy CaX molecular orbital. This conclusion is qualitatively supported by population analyses of two independent Hartree–Fock calculations which give 13%[16] and 18%[31] $4p\sigma$ character for the $X\,^2\Sigma^+$ state of CaF. Knight *et al.*[22] made similar s/p mixing conclusions for the $X\,^2\Sigma^+$ states of SrF and BaF. This latter result, however, was obtained from magnetic hfs associated with the ^{87}Sr and ^{137}Ba nuclei.

The CaBr and CaI $B\,^2\Sigma^+$ state mixing fractions (65%–55% $4p\sigma$, 35%–45% $3d\sigma$) are consistent with an independent estimate[32] of e^2, based on radiative lifetime data,[9] Λ doubling of the $A\,^2\Pi$ state, and the spin–rotation constant of the $B\,^2\Sigma^+$ state. Hartree–Fock calculations for CaF $B\,^2\Sigma^+$ give 38% $4p\sigma$, 54% $3d\sigma$[17] or 45% $4p\sigma$, 48% $3d\sigma$.[31]

TABLE VI. Mixing fractions from magnetic hfs.

	CaF	CaCl	CaBr	CaI
$g^2\,(X\,^2\Sigma^+)^a$	0.65	0.75	0.77	0.76
$e^2\,(B\,^2\Sigma^+)^b$	···	···	0.66	0.55

[a] g^2 is the fractional $4s\sigma$ character in $X\,^2\Sigma^+$; $(1-g^2)$ is $4p\sigma$.
[b] e^2 is the fractional $4p\sigma$ character in $B\,^2\Sigma^+$; $(1-e^2)$ is $3d\sigma$.

The Hartree–Fock calculations also indicate that the $B\,^2\Sigma^+$ state contains less than 7% $4s\sigma$ and the $X\,^2\Sigma^+$ state has less than 3% $3d\sigma$, justifying their exclusion from Eqs. (8a) and (8c).

The smaller magnetic hfs in the B than X states is explained by a simple cancellation effect. The $4p\sigma$ and $3d\sigma$ mixing coefficients are nearly equal in magnitude but opposite in sign; thus, the p and d orbital contributions to the hfs almost cancel. This is reasonable since the $4d\sigma$ orbital has a lobe that points directly at the halide, so it should be more heavily mixed. The negative signs for the mixing coefficients in Eqs. (8) are essential to enable the nonbonding Ca^+ orbital to distort so that it avoids the negatively charged X^-. The increase in spin density at the halide nucleus in the $X\,^2\Sigma^+$ states of the CaF to CaI series is due to an increase in the atomic orbital density $|\phi_{nsX^-}(0)|^2$ (from 11.4 a.u. for F to 22.9 for I[30]) and an increase in the overlap integral {from $S\,[4s\sigma(Ca^+),\, 2s\sigma(F^-)] = 0.219$ to $S\,[4s\sigma(Ca^+),\, 5s\sigma(I^-)] = 0.352$}.

Additional support for this interpretation comes from comparison with CaF, SrF, and BaF, where there is no question of covalent mixing. In this series, b/g_I is 20, 18, and 11 MHz, respectively.[22] The decrease in spin density from CaF to BaF is caused by decreasing spin polarization as measured by the metal-halide overlap integral {$S\,[5s\sigma(Sr^+),\, 2s\sigma(F^-)] = 0.113$ and $S\,[6s\sigma(Ba^+),\, 2s\sigma(F^-)] = 0.039$}. The calculated mixing fractions for the $X\,^2\Sigma^+$ states are 37% admixed $5p\sigma$ for SrF and only 4% $6p\sigma$ admixed for BaF. It seems likely that the small admixture of $6p\sigma$ in BaF is a reflection of the inability to calculate the small overlap integral accurately rather than a dramatic increase in the orbital purity of the ground state.

The electric quadrupole hyperfine structure can be rationalized similarly. The model is expected to work less well, however, since eQq values depend on the gradient of the charge density at the nucleus rather than simply on its magnitude. In addition, all filled orbitals contribute to eQq, thus vitiating the single orbital model adopted here. However, *differences* between eQq values for electronic states with all but one orbital in common should be consistent with a single orbital model.

In this model, it is the distortion of np halide orbitals by the presence of the unpaired Ca^+ electron that is important. Calculation of overlap integrals demonstrates that $4p\pi$ and $3d\pi$ Ca^+ orbitals have much greater overlap with halide np orbitals than $4s\sigma$, $4p\sigma$, or $3d\sigma$ Ca^+ orbitals. Thus, this qualitative picture predicts eQq for the $A\,^2\Pi$ state should have a larger absolute value than those for $X\,^2\Sigma^+$ and $B\,^2\Sigma^+$. This is the case for CaBr and CaI (Table V).

It is clear, however, that the model gives an unsatisfactory explanation of the electric quadrupole hfs except for possibly the ground $X\,^2\Sigma^+$ state. The $X\,^2\Sigma^+$ state is a reasonably pure $4s\sigma$ state. Using the mixing coefficients from the magnetic hfs, overlap integrals calculated as described above, and eQq_{nlm} values (Ref. 14, p. 579) for $l=1$, $m=0$, the eQq'' values are predicted to be -2 MHz for CaCl, 10 MHz for CaBr, and -150 MHz for CaI. Calculations using this simple model for the excited states predict very small eQq (~1 MHz) for both $A\,^2\Pi$ and $B\,^2\Sigma^+$ states of CaBr, mainly due to cancellation by $4p$ and $3d$ terms. These estimates are at variance with experimental ΔeQq values of Table V.

The size of $\Delta eQq(B-X)$ in CaBr and CaI is particularly puzzling. For CaBr, the eQq value of the B state is identical, within experimental error, to that of the ground state. In CaI, however, eQq of the B state is almost the same as that of the $A\,^2\Pi$ state. We can offer no reasonable explanation for this behavior. More sophisticated calculations are required to explain the electric quadrupole hfs for the excited states of the calcium halides.

V. CONCLUSION

The intermodulated fluorescence spectra of CaBr and CaI have provided some insight into the electronic structure of the calcium monohalide radicals. The data suggest that bonding is completely ionic for the CaX series. A simple model built from a small number of atomic orbitals has provided an explanation for the magnetic hyperfine structure. It is hoped that this work will encourage more accurate determinations of hyperfine structure in these molecules (particularly the Frosch and Foley[7] c parameters and eQq for the $X\,^2\Sigma^+$ states) by radio frequency methods.[17] Accurate molecular calculations of electronic properties of the alkaline earth halides would also be valuable. The hyperfine structure serves as a useful test of computed molecular wave functions.

ACKNOWLEDGMENTS

P. F. B. was supported, in part, by a National Sciences and Engineering Research Council of Canada postgraduate fellowship. This research was supported by the following grants: AFOSR-76-3056, NSF CHE-78-18427, NSF CHE-78-10178, and NATO 1177.

[1]M. S. Sorem and A. L. Schawlow, Opt. Commun. 5, 148 (1972).
[2]A. Muirhead, K. V. L. N. Sastry, R. F. Curl, Jr., J. Cook, and F. K. Tittel, Chem. Phys. Lett. 24, 208 (1974).
[3]R. S. Lowe, H. Gerhardt, W. Dillenschneider, R. F. Curl, Jr., and F. K. Tittel, J. Chem. Phys. 70, 42 (1979).
[4]J. M. Brown, H. Martin, and F. D. Wayne, Chem. Phys. Lett. 55, 67 (1978).
[5]P. F. Bernath, P. G. Cummins, and R. W. Field, Chem. Phys. Lett. 70, 618 (1980).
[6]A. S-C. Cheung, R. C. Hansen, A. M. Lyyra, and A. J. Merer (private communication).
[7]R. A. Frosch and H. M. Foley, Phys. Rev. 88, 1337 (1952).
[8]J. B. West, R. S. Bradford, J. D. Eversole, and C. R. Jones, Rev. Sci. Instrum. 46, 164 (1975).
[9]P. J. Dagdigian, H. W. Cruse, and R. N. Zare, J. Chem. Phys. 60, 2330 (1974).
[10]S. Gerstenkorn and P. Luc, *Atlas du spectre d'absorption de la molecule d'iode* (CNRS, Paris, 1978).
[11]P. F. Bernath, R. W. Field, B. Pinchemel, Y. Lefebvre, and J. Schamps, J. Mol. Spectrosc. (unpublished).
[12]D. E. Reisner, P. F. Bernath, and R. W. Field, J. Mol. Spectrosc. (unpublished).
[13]T. M. Dunn, in *Molecular Spectroscopy: Modern Research*, edited by K. N. Rao and C. W. Mathews (Academic, New York, 1972), p. 231.
[14]W. Gordy and R. L. Cook, *Microwave Molecular Spectra*, Part II of *Chemical Application of Spectroscopy*, edited by W. West (Wiley, New York, 1970).
[15]H. E. Radford, Phys. Rev. 136, 1571 (1964). Note there are several factor of 2 errors in his expression for hfs in $^2\Sigma$ states. The one relevant to this paper is that W_Q should have a term $3C(C+1)/4$.
[16]W. J. Childs, G. L. Goodman, and L. S. Goodman, J. Mol. Spectrosc. (unpublished).
[17]W. J. Childs and L. S. Goodman, Phys. Rev. Lett. 44, 316 (1980).
[18]A. Yokozeki and J. S. Muenter, J. Chem. Phys. 72, 3796 (1980).
[19]J. V. Martinez de Pinillos and W. Weltner, Jr., J. Chem. Phys. 65, 4256 (1976).
[20]P. B. Ayscough, *Electron Spin Resonance in Chemistry* (Methuen, London, 1967), p. 438.
[21]A. J. Freeman and R. E. Watson, Phys. Rev. Lett. 6, 343 (1961).
[22]L. B. Knight, Jr., W. C. Easley, W. Weltner, Jr., and M. Wilson, J. Chem. Phys. 54, 322 (1971).
[23]G. Burns, J. Chem. Phys. 41, 1521 (1964).
[24]E. A. Boudreaux, L. C. Cusachs, and L. Dureaux, *Numerical Tables of Two-Centre Overlap Integrals* (Benjamin, New York, 1970).
[25]G. Herzberg, *Spectra of Diatomic Molecules* (Van Nostrand, Princeton, N.J., 1950), p. 374.
[26]E. S. Rittner, J. Chem. Phys. 19, 1030 (1951).
[27]P. D. Kleinschmidt and D. L. Hildenbrand, J. Chem. Phys. 68, 2819 (1978).
[28]P. F. Bernath and R. W. Field, J. Mol. Spectrosc. 82, 339 (1980).
[29]R. N. Zare, A. L. Schmeltekopf, W. J. Harrop, and D. L. Albritton, J. Mol. Spectrosc. 46, 37 (1973).
[30]C. Froese-Fischer, At. Data 4, 301 (1972).
[31]B. Pouilly and J. Schamps (private communication).
[32]P. Bernath, Ph.D. thesis, 1980.